Experimental Thermal and Fluid Science 39 (2012) 252–264

Contents lists available at SciVerse ScienceDirect

Experimental Thermal and Fluid Science

journal homepage: www.elsevier.com/locate/etfs

An experimental study on aerodynamics of NACA2415 aerofoil at low Re numbers

M. Serdar Genç [a,*], İlyas Karasu [a,b], H. Hakan Açıkel [a]

[a] Wind Engineering and Aerodynamics Research Laboratory, Department of Energy Systems Engineering, Erciyes University, 38039 Kayseri, Turkey
[b] İskenderun Civil Aviation School, Mustafa Kemal University, 31200 İskenderun, Hatay, Turkey

ARTICLE INFO

Article history:
Received 13 September 2011
Received in revised form 20 January 2012
Accepted 23 January 2012
Available online 2 February 2012

Keywords:
Low Reynolds number
Transition
Laminar separation bubble
Hot-wire anemometry
Oil flow visualization

ABSTRACT

This study is a detailed experimental investigation on aerodynamics of a NACA2415 aerofoil by varying angle of attack from −12° to 20° at low Reynolds number flight regimes (0.5×10^5 to 3×10^5). For this investigation, pressure distributions over the aerofoil were measured using a system including a pitot-static tube, a scanivalve unit and a pressure transducer. Moreover, time-dependant lift and drag forces and pitch moment of the aerofoil were obtained by using an external three-component load-cell system. Velocity measurements at different points over the aerofoil were carried out by using a hot-wire anemometer, and oil flow visualization method was used to photograph the surface flow patterns. The experimental results showed that as the angle of attack increased, the separation and the transition points moved towards the leading edge at all Reynolds numbers. Furthermore as the Reynolds number increased, stall characteristic changed and the mild stall occurred at higher Reynolds numbers whereas the abrupt stall occurred at lower Reynolds numbers. The stall angle varied with Re number due to the viscous effects and decreased with decreasing Re number. By the decreasing of the Re number, short bubble burst at higher angles of attack, which caused long bubble to occur.

1. Introduction

Low Reynolds (Re) number aerodynamics has gained more attention due to increasing applications of Unmanned Air Vehicle (UAV), Micro Air Vehicle (MAV) and wind turbine. At low Reynolds number flows, laminar separation bubble may cause negative effects, such as decreasing on lift, increasing on drag, reducing stability of the aircraft, vibration, and noise [1–3]. It is important to understand the behavior of laminar separation bubbles (LSBs) to design a control system of LSB and to compose a new aerofoil which is no affected from LSB. Gaster [4] performed an experimental study about LSB by using hot-wire anemometer and oscilloscope. This study was carried out over a wide range of Re numbers and in a variety of pressure distributions. The bursting circumstances of short bubbles were determined by a unique relationship between Re number and pressure rise. Consequently, LSB was classified as short and long bubble just as Tani [5] did. Tani showed that when Re number was decreased the short bubble burst at higher angles of attack, and that caused long bubble or unattached flow to occur. Rinioie and Takemura [6] carried out an experimental investigation on NACA0012 aerofoil at $Re = 1.35 \times 10^5$. They obtained that the short bubbles formed at which angle of attack was less than 11.5°, the long bubbles occurred at which angle of attack was more than 11.5°. Tan and Auld [7] studied experimentally on Wortmann FX67-150K aerofoil at low Reynolds numbers. They concluded that as the Re number and turbulence intensity of the freestream increased, earlier transition occurred and this caused length of LSB to shorten. Sharma and Poddar [8] conducted on an experimental investigation about the formation of LSB and transition process on NACA0015 aerofoil by varying the angle of attack from −5° to 25° at low Re numbers. In this study, the flow visualizations were done by using oil flow technique for qualitative analysis of the transition zone. It was resulted that as the angle of attack was increased the separation bubble moved towards the leading edge of the aerofoil and then bursted at a particular angle of attack, and the bubble bursting caused abrupt stall to occur. Ricci et al. [1,2] studied on formation and controlling LSB which occurred on the upper surface of aerodynamic bodies at low Reynolds number. The experiments were carried out to get the locations of the laminar bubble characteristic points (separation, transition and reattachment points) with and without the acoustic disturbance. The frequency range of the acoustic force was between 200 and 800 Hz with a step of 100 Hz was inspected. They presented that a sinusoidal sound wave having determined frequency reduced the laminar bubble longitudinal dimensions retarding the separation and anticipating the reattachment.

Diwan and Ramesh [9] investigated experimentally the length and height of the LSB on a flat plate at different Re numbers. It was obtained that both length and height of the LSB decreased,

* Corresponding author. Tel.: +90 352 2076666 32132; fax: +90 352 4375784.
E-mail addresses: musgenc@erciyes.edu.tr (M.S. Genç), ikarasu@mku.edu.tr (İ. Karasu), halilhakanacikel@gmail.com (H. Hakan Açıkel).

0894-1777/$ - see front matter © 2012 Elsevier Inc. All rights reserved.
doi:10.1016/j.expthermflusci.2012.01.029

Nomenclature

c	chord length (m)
b	span length (m)
α	angle of attack (°)
D	drag force (N)
L	lift force (N)
M	moment force (N)
U_∞	freestream velocity (m/s)
u'	velocity fluctuation (m/s)
ρ	density of air (kg/m^3)
μ	dynamic viscosity of air (Ns/m^2)
P_∞	freestream pressure (Pa)
P	local pressure (Pa)
Re	Reynolds number $(\rho * (U_\infty) * c)/\mu)$
P_{dyn}	reference dynamic pressure $(0.5 * \rho * (U_\infty)^2)$
C_P	pressure coefficient $(P - P_\infty)/(0.5 * \rho * (U_\infty)^2)$
C_D	drag coefficient $D/(0.5 * \rho * (U_\infty)^2 * b * c)$
C_L	lift coefficient $L/(0.5 * \rho * (U_\infty)^2 * b * c)$
C_M	moment coefficient $M/(0.5 * \rho * (U_\infty)^2 * b * c^2)$
x/c	ratio of the position on aerofoil with chord length
L_b	bubble length
X_s	separation point
X_t	transition point
X_r	reattachment point
U_{Re}	uncertainty of Reynolds number
U_{C_P}	uncertainty of pressure coefficient
U_{C_L}	uncertainty of lift coefficient
U_{C_D}	uncertainty of drag coefficient
U_{C_M}	uncertainty of moment coefficient

Fig. 1. Photograph of the experimental set-up.

and reducing ratio of the length is more than that of the height as Re number was risen. Yang et al. [10] carried out an experimental study about LSB over GA (W)-1 aerofoil at different low Reynolds number. It was resulted that while maximum length of the bubble was 20% of the chord length, the maximum height of the bubble was only 1% of the chord length. Furthermore, they showed that at more than angles of attack of 7° Kelvin-Helmholtz instabilities caused unsteady vortexes caused by LSB. Hain et al. [11] presented dynamics of LSBs at low-Reynolds-number aerofoils. It was found that Kelvin-Helmholtz instabilities had a weak coherence in the spanwise direction, and in a later stage of transition these vortices led to a three-dimensional breakdown to turbulence. Burgmann et al. [12] studied experimentally on the flow over SD7003 aerofoil used in wind turbine blades at low Re numbers. They concluded that vortex roll-up which was initialized by Kelvin-Helmholtz instability played effective role at transition process. Haggmark et al. [13] conducted experimental and numerical investigation on transitional separation bubble over elliptical leading edged flat plate. The flow was modelled numerically using engineering transition prediction methods and two-dimensional direct numerical simulations (DNS). They found that low-amplitude two-dimensional instability waves leaded to transition, and e^N method gave a result in accordance with experiments and DNS. Lang et al. [14]

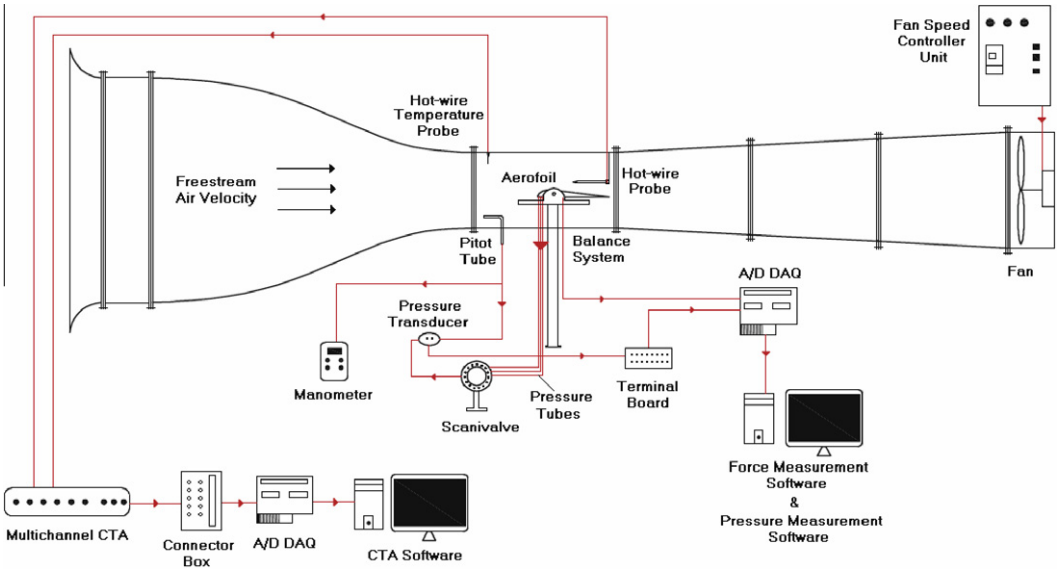

Fig. 2. Schematic diagram of the experimental set-up.

Fig. 3. Manufacturing processes and aerofoil models manufactured with end-plate.

Table 1
Uncertainties as % in pressure coefficient (U_{C_P}), lift force coefficient (U_{C_L}), drag force coefficient (U_{C_D}), pitch moment coefficient (U_{C_M}) and Reynolds number (U_{Re}).

Reynolds number	U_{C_P}	U_{C_L}	U_{C_D}	U_{C_M}	U_{Re}
50,000	6.6	5.6	6.4	7.0	5.5
100,000	5.3	5.0	5.2	6.1	4.7
200,000	4.6	4.5	4.4	5.5	4.0
300,000	–	4.0	3.5	4.3	3.2

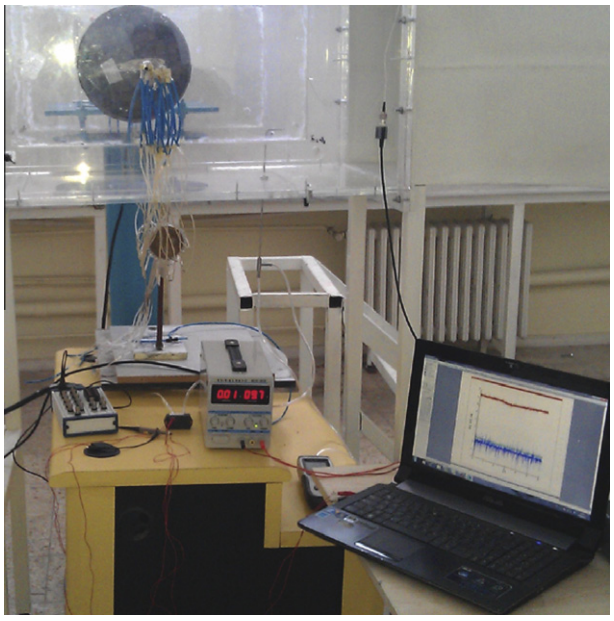

Fig. 4. Experimental set-up for pressure measurements over NACA2415 aerofoil.

also carried out an experimental and numerical study about transition development in a separation bubble over elliptical leading edged flat plate. They showed that transition in LSB was driven by amplification of 2-D Tollmien/Schlichting waves and first stages of the 3-D disturbances played minor role in the transition. Moreover, the results showed that bidirectional vortexes lead to 3D breakdown. Brandt et al. [15–18] studied experimentally and numerically about effect of free-stream turbulence on the transition. The numerical results indicated important similarities with the flow structures in experimental studies on the secondary instability and breakdown of steady symmetric streaks. They concluded that the transition location moved to lower Reynolds numbers by increasing the integral length scale of the free-stream turbulence. Genç et al. [19–23] tested the behavior of the turbulence and transition models in the study of prediction of the LSB over the aerofoils at low and high Re numbers, and in the study of

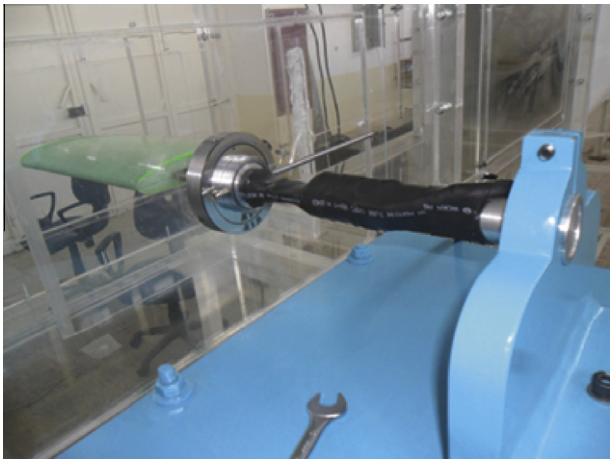

Fig. 5. Experimental set-up for the force measurements.

controlling this LSB by using high lift, blowing and suction systems. The numerical results of the turbulence models indicated varying degrees of success in predicting the boundary layer flow field and the separation bubble, while the results of transition models accurately predicted the location and extent of the separation bubble in the single element aerofoil cases. In the control cases, it was predicted that the separation bubble was eliminated by using the slat, blowing and suction resulting in some marginal increase in the lift and decrease in drag.

The aim of this study is to evaluate aerodynamic performance of a NACA2415 aerofoil at the angles of attack from -12° to 20° at Re numbers of 0.5×10^5, 1×10^5, 2×10^5 and 3×10^5. Moreover, due to the fact that flow regime is low Re number flow, the LSB, transition and reattachment are important and their effects on aerodynamic performance is considered.

2. Experimental apparatus and methods

2.1. Wind tunnel and models

The experiments were carried out in a low-speed, suction-type wind tunnel with a square working section of 500 mm × 500 mm located at the Department of Energy Systems Engineering, University of Erciyes. The ratio of cross sectional area of contraction cone was 9:1 and the side walls of the working section were expanded with a divergence angle of 0.3° on each side to minimize boundary layer effects on the working section walls, and to give a constant static pressure. Maximum speed near center of the working section was about 40 m/s, free-stream turbulence intensity at maximum speed was about 0.3%; about 0.7% at lowest speed (5 m/s) [24].

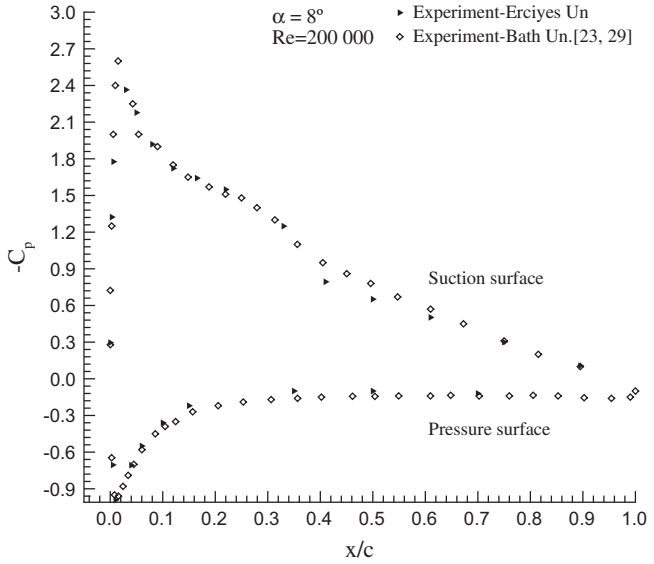

Fig. 8. Comparison of C_p distributions over the NACA2415 aerofoil in present study (Erciyes University) and the study in University of Bath [23,29] (Re = 2×10^5, $\alpha = 8^\circ$).

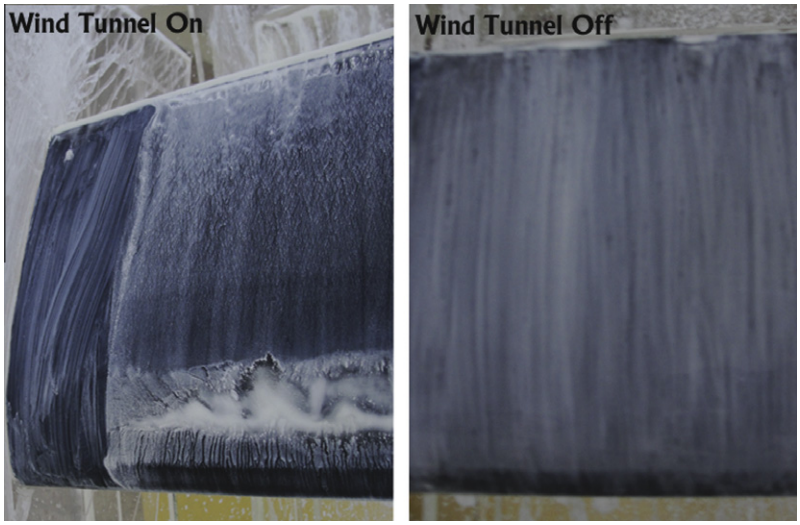

Fig. 6. Sample of oil-flow visualization experiment over NACA2415 aerofoil on which oil laid.

Fig. 7. Constant temperature anemometry system and the probe over the NACA2415 aerofoil.

The experiments were carried out at Reynolds (Re) numbers of 0.5×10^5, 1×10^5, 2×10^5 and 3×10^5 based on chord length of aerofoil (c) and free-stream velocity (U_∞). The experimental setup and schematic diagram are shown in Figs. 1 and 2.

The aerofoil models were manufactured out of glass fiber and two component epoxy resin covering up NACA2415 foam aerofoil using a steel mold (Fig. 3). Epoxy resin was mixed carefully with epoxy hardener at a certain rate (5:1) according to the manufacturers directions. After a thin mixed epoxy layer was applied on the NACA2415 foam which was prepared using a hot-wire and two wood aerofoils, glass fiber covered up NACA2415 foam. The remaining layers of glass fiber were laid onto the previous layers successively in a similar way. Later, NACA2415 foam covered up with glass fiber and epoxy resin located in the NACA2415 steel mold. The aerofoil in the mold was left to solidify for 8–12 h at room temperature. The edges of the solidified composite aerofoil was shaved to obtain clean plate edges and approximate the NACA2415 profile definition within an accuracy of 0.1 mm. The composite plates were left at room temperature for three days to complete the curing period and to reach the maximum strength. Later, plexi-glass end plates were assembled to two side of aerofoil. The manufactured aerofoils have a span length of 290 mm, and a chord length of $c = 180$ mm.

The uncertainty of the measurement depends on the uncertainties of the calibration device, linearization, repeatability, the accuracy of reference calibration device, position of the probe, air density, ambient pressure, etc. The uncertainty of the velocity measurement using hot-wire anemometry and the pressure measurement using pressure transducer were determined as 4.0% and 4.6% for Re = 200,000, respectively. The uncertainty values in the pressure coefficient (U_{C_P}), lift force coefficient (U_{C_L}), drag force coefficient (U_{C_D}), pitch moment (U_{C_M}) and Reynolds number (U_{Re}) were given in Table 1.

Blockage ratio of NACA2415 at the angle of attack of 0° in our wind tunnel was $0.18 \times 0.15 \times 0.29/(0.5 \times 0.5) = 0.031$ (~3%). Blockage ratio of NACA2415 at the angle of attack of 20° was 0.071(~7%). The blockage corrections are not made on the experimental results, because the blockage effects on the experimental results are negligible when the blockage ratio is less than 10% [25,26].

2.2. Pressure measurements

For the measurement of pressure distributions of suction and pressure surfaces on the NACA2415 aerofoil, a system including a pitot-static tube, a scanivalve unit, a pressure transducer and 24 pressure tappings of 0.8 mm in diameter, which are flush along the mid-span of the upper and lower surfaces of the wing was used (Fig. 4). Pressure measurements were carried out by using a computer-controlled data acquisition system. The pressure was measured by using Honeywell 163PC01D75 model differential pressure transducers with a pressure range of 623 Pa. Calibration of the pressure transducer was made by using CEM DT-8920 manometer and Kimo TPL-03–300 pitot tube with an accuracy of

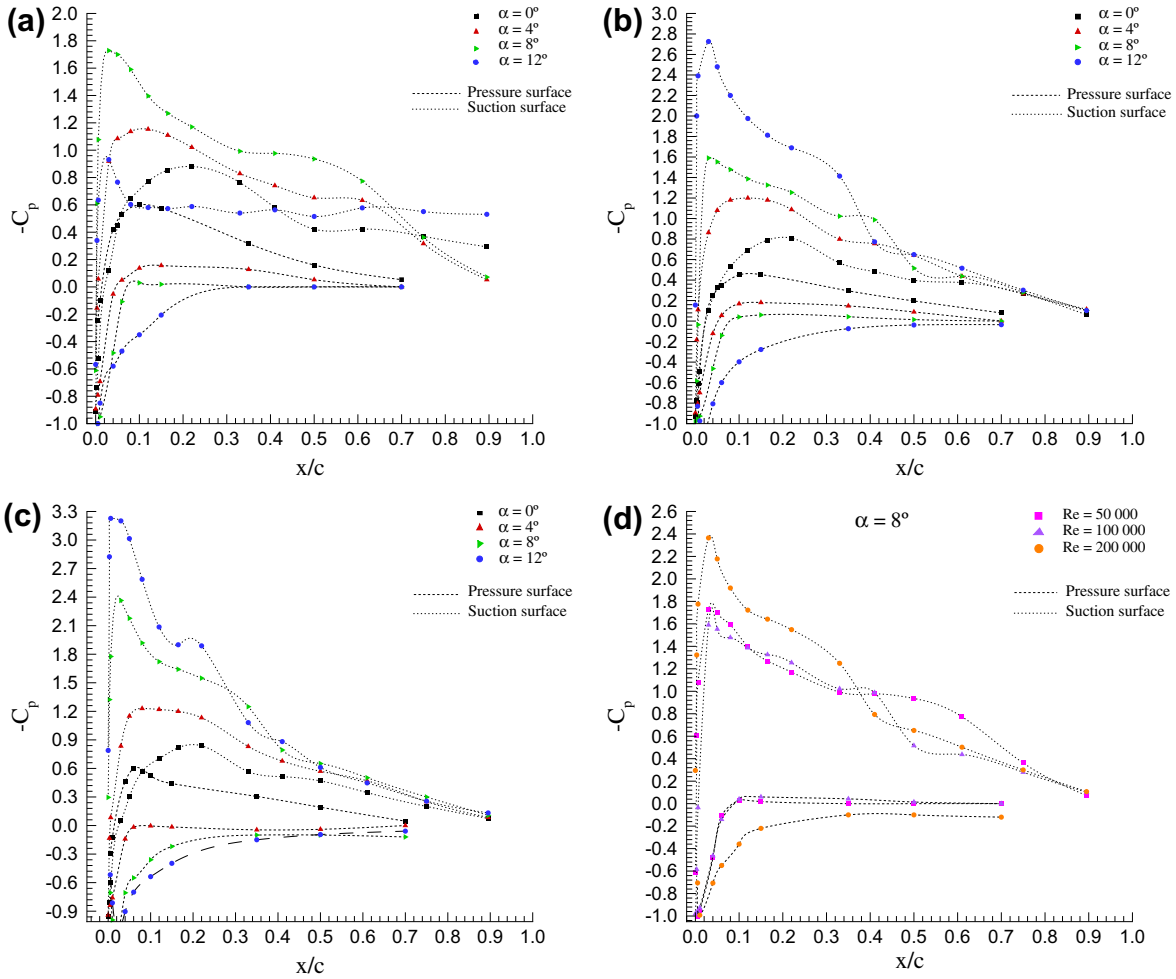

Fig. 9. C_p distributions over the NACA2415 aerofoil (a) Re = 0.5×10^5, (b) Re = 1.0×10^5, (c) Re = 2×10^5, and (d) $\alpha = 8°$.

1 Pa. The maximum response time of the pressure transducer was about 1 ms. The pressure signals were acquired at a sampling rate of 1000 samples per second and each of the mean pressures was obtained by means of averaging 16,384 data points for over 16.4 s. A software was written in C programming language to acquire signals in conjunction with a 16-bit A/D converter, and final post-processing was complemented in MATLAB to calculate the mean pressure distributions. Experiments were conducted over a range of angles of attack in order to calculate the pressure coefficient distribution.

2.3. Force measurements

An external three-component load-cell system was used for measuring the lift and drag forces and moment on the aerofoil. The MSM balance system (Fig. 5) software lets the calibration of forces and moment, and gives digital output of the lift and drag forces in N and moment in Nm; it was calibrated regularly for forces and moment measurements and its linearity was ensured in the range of interest. The calibration was performed by loading the load cell with known weights. Calibration was repeated before each set of experiments to ensure consistency. Sets of data chosen at random were repeated. The maximum lift and drag forces and moment of the system were 110 N, 50 N and 10 Nm, respectively. The force data was collected at a sampling frequency of 1000 Hz over 120 s. Mean forces and moment and its coefficients were calculated using Microsoft Excel Software.

2.4. Oil flow visualization

Oil flow visualization is a simple and effective way of scrutinizing surface flow events. In order to photograph the surface flow events using this method, the pigmented oil is painted onto a mat black aerofoil surface (Fig. 6) and the wind tunnel is run. Once it has dried, the painted and patterned surface can be photographed. It is important that the type of oil mixture which would work at the speed of the wind tunnel. The mix should have the right consistency to effectively indicate the development of the boundary layer. Furthermore, the inertia forces of the moving oil should be lower than the viscous and surface tension forces [27] in order to not affect the conditions at the surface. Kerosene, light diesel oil and light transformer oil are most common oils, and titanium dioxide, china clay and fluorescent chrysene are most common pigments [27]. Furthermore, oleic acid can be added to the mixture to clearly see the pigment deposit on the oiled surface. The simplest mix to make was kerosene, titanium dioxide and a very small amount of oleic acid: the ratio of kerosene to oleic acid was roughly 20:1 [28] and this ratio of mixture was used in the present study (Fig. 6). However, the pigment was added in some doses based on Reynolds number.

2.5. Velocity measurements

Velocities and turbulence intensities at different points from the leading edge towards the trailing edge ($x/c = 0.05, 0.1,$

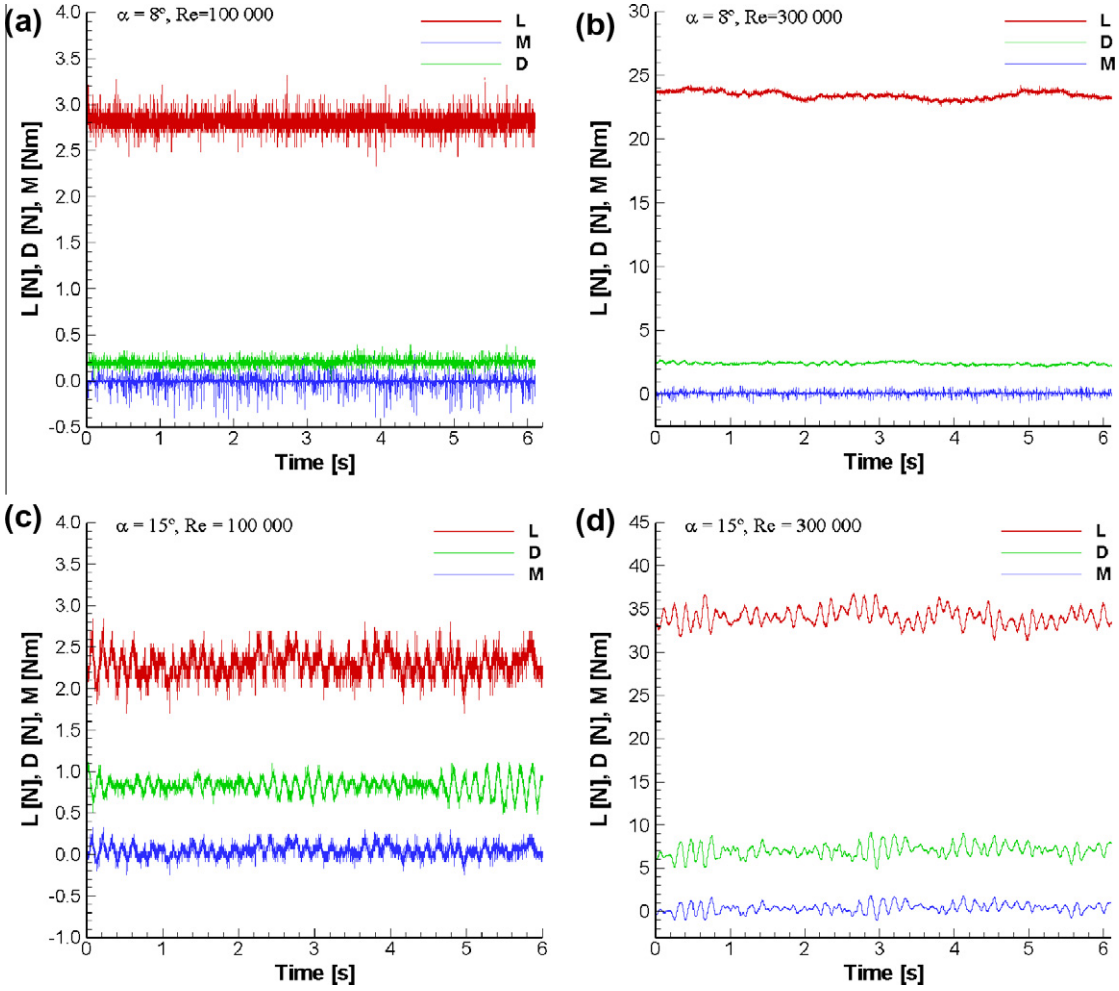

Fig. 10. Time-dependent forces and moment variations over the NACA2415 aerofoil for $\alpha = 8°$ at (a) $Re = 1 \times 10^5$, (b) $Re = 3 \times 10^5$ for $\alpha = 15°$ at (c) $Re = 1 \times 10^5$, and (d) $Re = 3 \times 10^5$.

0.2, . . . , 0.7) over the NACA2415 aerofoil were measured by using Dantec Dynamics Multichannel (6 Channels and System Temperature and Velocity Probe Channels) Constant Temperature Anemometer (54N81) by using 55P15 and 55P16 single wire probes (Fig. 7). x/c is the ratio of the distance from leading edge of the aerofoil with the chord length. The anemometer has a frequency bandwidth up to 250 kHz. The calibration of the probes was done by using the pitot-static tube and the manometer using a fourth-order polynomial curve fitting with linearization errors between −1.1% and 1.2% from the calibration data [24]. At each velocity measurement point, 16,384 velocity values were acquired with a sampling rate of 2 kHz with a low-pass filter setting of 1 kHz. Thus, the measuring time corresponded to 8 s. The frequency variations depending on velocity fluctuations were determined from the power spectrum analysis of the velocities over the NACA2415 aerofoil using MATLAB. The probe was located at 2–5 mm upstream above the upper surface of the NACA2415 aerofoil using metal bar on the lids of wind tunnel working section (Fig. 7). The closest spacing between the probe and the aerofoil was 2 mm. As the Re number and the angle of attack increased, the spacing was widened to protect the probe from contact with the rising and vibrating aerofoil which was fixed to one side of the tunnel test section.

3. Experimental results

3.1. Pressure coefficients

Firstly, measurements of the pressure distribution were taken under the same flow conditions as the experiments at $Re = 2 \times 10^5$ and $\alpha = 8°$ in University of Bath, UK [22,23,29] to compare with the present study. The pressure coefficients were calculated from the pressure readings obtained from the pressure tappings at many points across the aerofoil surface and the pitot-static tube. As can be seen from Fig. 8, 33 pressure tappings were used in the experiments at the University of Bath whereas 24 pressure tappings were used in this study. The uncertainty of the pressure coefficient in University of Bath was about 3.5%. Finally, although there are little differences due to the experimental uncertainty, there is a quite good agreement between both experiments.

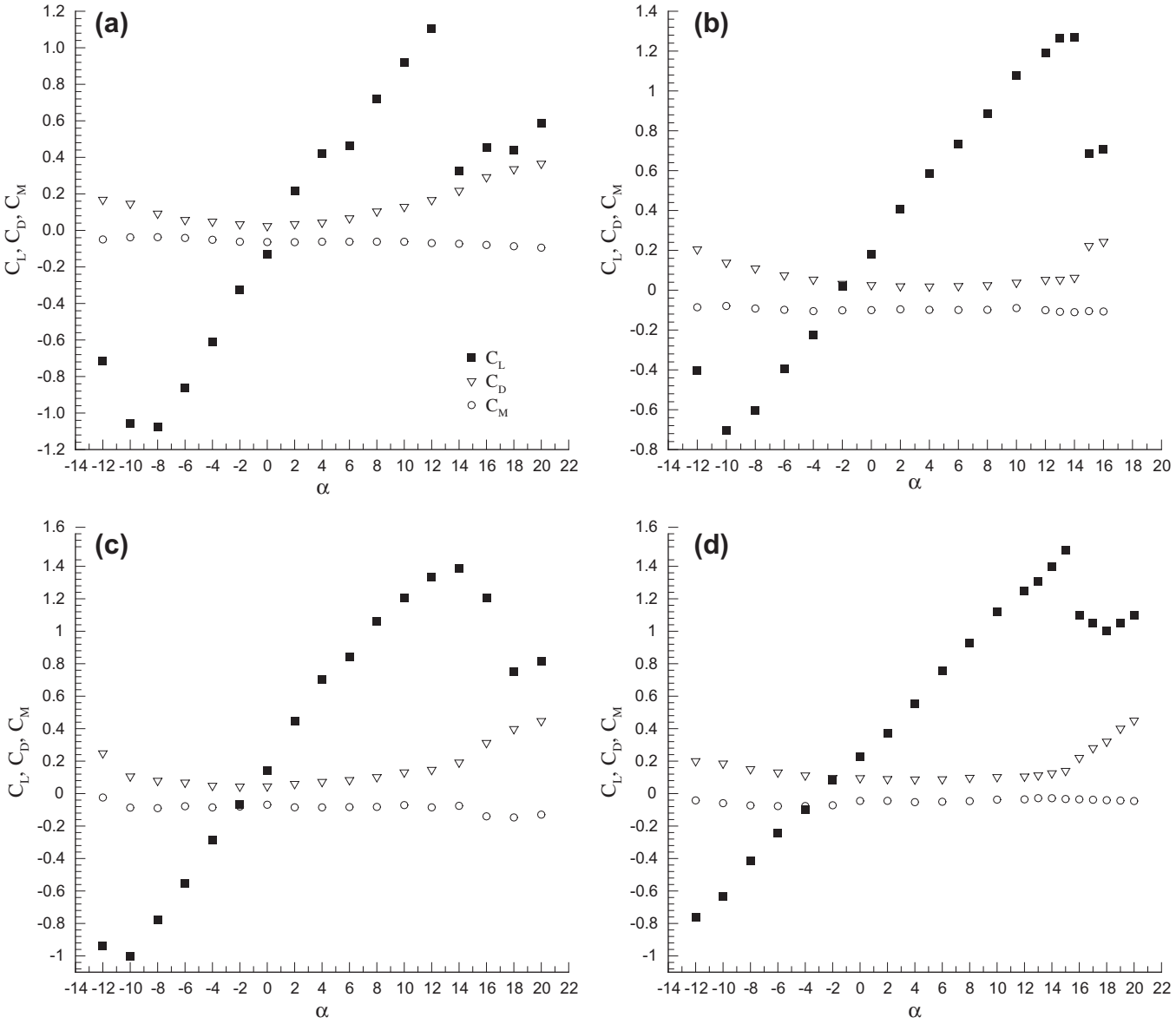

Fig. 11. Aerodynamics coefficients of the NACA2415 aerofoil versus the angle of attack (a) $Re = 0.5 \times 10^5$, (b) $Re = 1 \times 10^5$, (c) $Re = 2 \times 10^5$, and (d) $Re = 3 \times 10^5$.

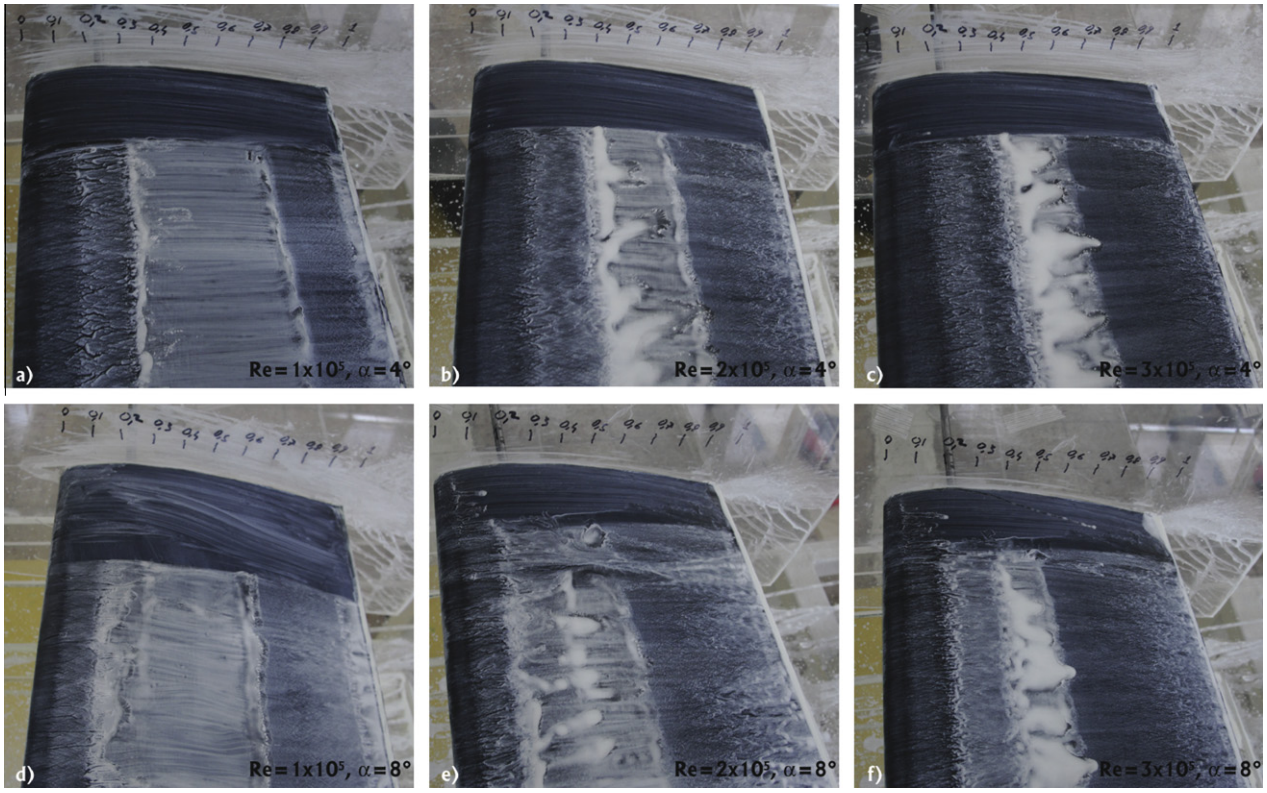

Fig. 12. The photographs of oil-flow visualization experiments over the NACA2415 aerofoil for $\alpha = 4^\circ$ (a) $Re = 1 \times 10^5$, (b) $Re = 2 \times 10^5$, (c) $Re = 3 \times 10^5$, for $\alpha = 8^\circ$, (d) $Re = 1 \times 10^5$, (e) $Re = 2 \times 10^5$ and (f) $Re = 3 \times 10^5$.

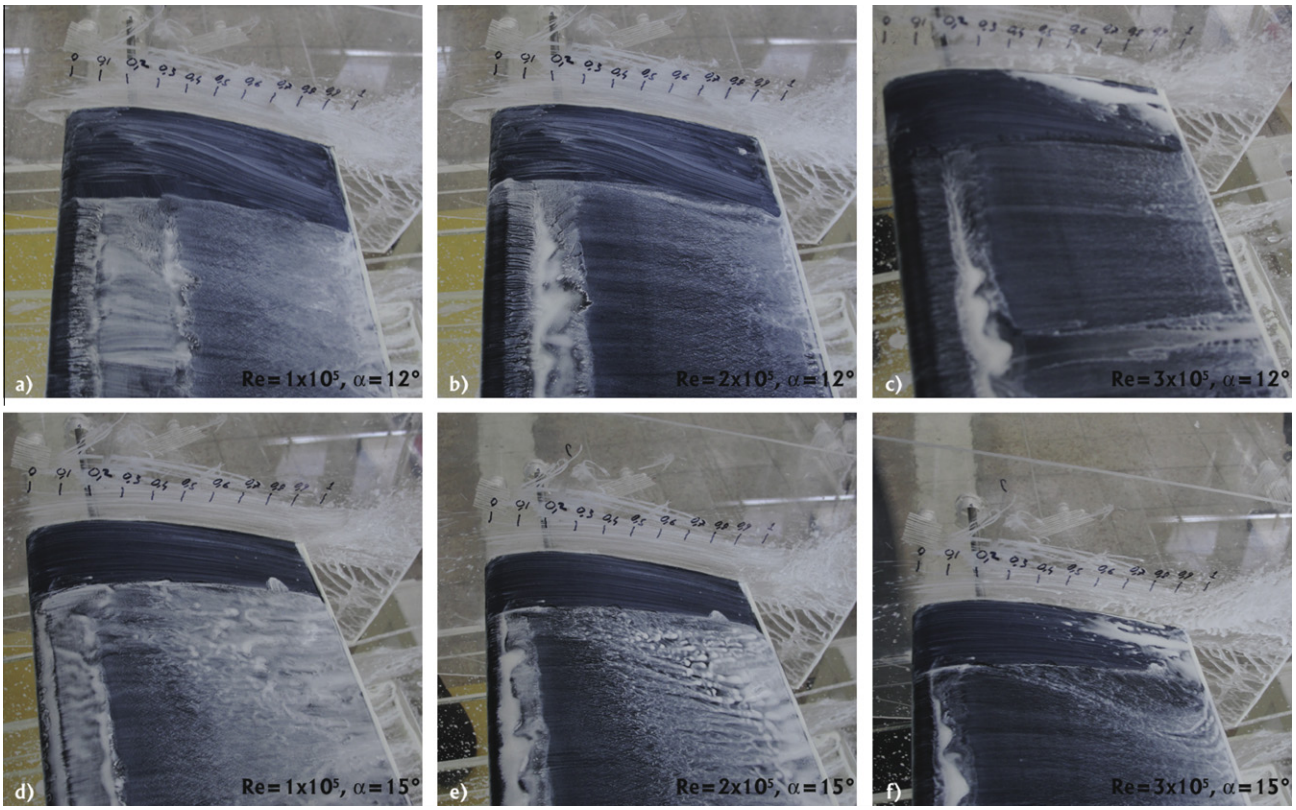

Fig. 13. The photographs of oil-flow visualization experiments over the NACA2415 aerofoil for $\alpha = 12^\circ$ (a) $Re = 1 \times 10^5$, (b) $Re = 2 \times 10^5$, (c) $Re = 3 \times 10^5$, for $\alpha = 15^\circ$, (d) $Re = 1 \times 10^5$, (e) $Re = 2 \times 10^5$, and (f) $Re = 3 \times 10^5$.

In order to show the evolution of the pressure and location of the separation bubble as the angle of attack and Reynolds number were increased, the graphs of pressure distribution (C_p) over the NACA2415 aerofoil at angles of $\alpha = 0°$, 4°, 8°, 12° at $Re = 0.5 \times 10^5$, 1×10^5, 2×10^5 were given in Fig. 9. In general these plots illustrate the development of the boundary layer as the pressure slowly increases after peak suction from the leading-edge to the trailing-edge. Furthermore, investigation of the distributions of pressure coefficients provides to see the formation and progress of the LSB, transition and re-attached flow. A slight increase and subsequent decrease in the curve of the pressure coefficient of suction surface in Fig. 9 point out the separation of the flow due to a high adverse pressure gradient and reattachment of the flow, respectively. Also, the transition from laminar to turbulent occurs just after the highest point of the peak in the curve of pressure coefficients of suction surface. The flow overcomes the adverse pressure gradient with the increase in the turbulent kinetic energy after the transition, and a subsequent turbulent reattachment takes place. However, the experiments of pressure distribution may not be able to show clearly the separation and reattachment points due to the fact that the pressure tappings can not be completely flush along the mid-span of the pressure and suction surfaces of the aerofoil. Consequently, as the angle of attack and Reynolds number increase the position of the pressure peak along the chord over suction surface of the NACA2415 aerofoil changes, and the LSB comes closer to the leading edge, and bubble size decreases.

3.2. Aerodynamics forces and coefficients

Time-dependent forces and moment variations over the NACA2415 aerofoil for $\alpha = 8°$ and $\alpha = 15°$ at different Re numbers are given in Fig. 10. Fluctuations in the curves of forces and moment at low Re numbers are more intense than the fluctuations of curves at high Re numbers due to the viscous effects. In the Fig. 10d, the moderate fluctuations in the forces and moment curves at the angle of attack of $\alpha = 15°$ and $Re = 3 \times 10^5$ point out the vortex formations at pre-stall. As seen in Fig. 10b the fluctuations in the forces and moment curves are not intense, but in Fig. 10d the fluctuations in the forces and moment curves are intense so this situation points out the beginning of the stall condition whereas in Fig. 10c the intense fluctuations in the forces and moment curves indicate post-stall condition. In addition, the presence of the stall condition owing to have a sharp decrease in C_L and increase in C_D after the angle of attack of 14 in Fig. 11b supports the intense fluctuations in the forces and moment curves in Fig. 10c.

Fig. 11 shows the values of C_L,C_D and C_M versus the angle of attack. Typical C_L–α curve for any Re number has a number of important features, as shown in Fig. 11. For lower angles of attack, the C_L–α curve is nearly linear, and very closely matches the one predicted by any theory such as a potential-flow theory, a panel method, RANS method, LES method, etc. due to attached flow. At higher values of α, the flow can no longer follow the upper surface of the aerofoil and becomes detached. There is a region above the upper surface, near the trailing edge, where the velocity is low and the flow reverses direction in places in a turbulent motion. This phenomenon is trailing edge separation. As the angle of attack is increased further, the beginning of the region of separated flow (trailing edge separation) moves towards the leading edge of the aerofoil. At a critical angle of attack, the lift component of the aerodynamic force falls off rapidly and the drag component increases rapidly as shown from C_L–α and C_D–α curves in Fig. 11. This phenomenon is called stall, and this critical angle of attack is called stall angle. The maximum lift coefficient defines the angle at which the aerofoil will stall and this is shown to vary with Reynolds number due to the viscous effects. As shown in Fig. 11, the stall occurred at angles of attack of 12°, 13°, 14° and 15° with $C_{Lmax} = 1.10$, 1.26, 1.38 and 1.5 at $Re = 0.5 \times 10^5$, 1×10^5, 2×10^5 and 3×10^5, respectively. This figure demonstrates that at lower Reynolds numbers the aerofoil stalls at lower angles of attack. This is due to the fact that at lower Reynolds numbers the aerofoil has a greater laminar boundary layer which does not overcome the adverse pressure gradient as well as a turbulent boundary layer would at the same angle of attack, and consequently trailing edge separation occurs sooner.

Moreover, as obtained in Tani's study [5], it was showed that the stall occurred more abruptly as Re number decreased. It was concluded that the mild stall occurred at higher Re numbers whereas the abrupt stall occurred at lower Re numbers.

Table 2
The separation (X_s), transition (X_t) and reattachment (X_r) points and bubble length (L_b) as x/c obtained from the results of the oil-flow visualization and pressure coefficient experiments.

Re number	α (°)	X_s	X_t	X_r	L_b
100,000	4	0.30	0.62	0.72	0.42
	8	0.20	0.45	0.60	0.40
	12	0.12	0.30	0.42	0.30
	15	0.05	0.15	0.20	0.15
200,000	4	0.35	0.62	0.66	0.31
	8	0.18	0.38	0.48	0.30
	12	0.15	0.25	0.30	0.15
	15	0.04	0.10	0.15	0.11
300,000	4	0.35	0.53	0.60	0.25
	8	0.30	0.35	0.45	0.15
	12	0.15	0.20	0.28	0.13
	15	0.05	0.08	0.15	0.10

3.3. Oil flow visualization results

In order to understand the concept of LSB, transition and boundary layer separation, oil flow visualization was applied to the upper surface of the aerofoil at angles of attack of 4°, 8°, 12° and 15° as seen from Figs. 12 and 13. The dense area of pigment shows where the flow has decelerated, which correlates with the point at which the pressure gradient cancels out causing separation. Looking at all four angles of attack, it is clear that as the angle of attack increases the separation point moves towards the leading edge at all Re numbers: for 4° (Fig. 12a) this occurs at 30% chord, 8° (Fig. 12d) at 20% chord, 12° (Fig. 13a) at 12% chord and for 15° (Fig. 13d) at 5% chord at $Re = 1 \times 10^5$. Furthermore, the separation (X_s), transition (X_t) and reattachment (X_r) points as percent of the chord and bubble length (L_b) as x/c obtained from the results of the oil-flow visualization and pressure coefficient experiments can be seen in Table 2. Not only the photographs indicated the progression of the separation point from 35% to 15% and finally 5% of the chord respectively, it also brought to light the possibility of a separation bubble shortly as the Re number increases. Investigation of the oil-flow visualization allows us to see the formation and progress of the separation bubble and re-attached flow, as observed in the pressure distribution graphs.

3.4. Hot-wire measurements

Fig. 14 shows time-dependent velocity fluctuations over the NACA2415 aerofoil at different points for different Re numbers and the angles of attack. In these figures, y axes indicates the velocity fluctuations, not velocity values. The velocity varies very little in the laminar flow region, while it has wider fluctuations in the turbulent flow. Transitional flow is a mixture of laminar and turbulent flow and in the transitional region velocity fluctuations make

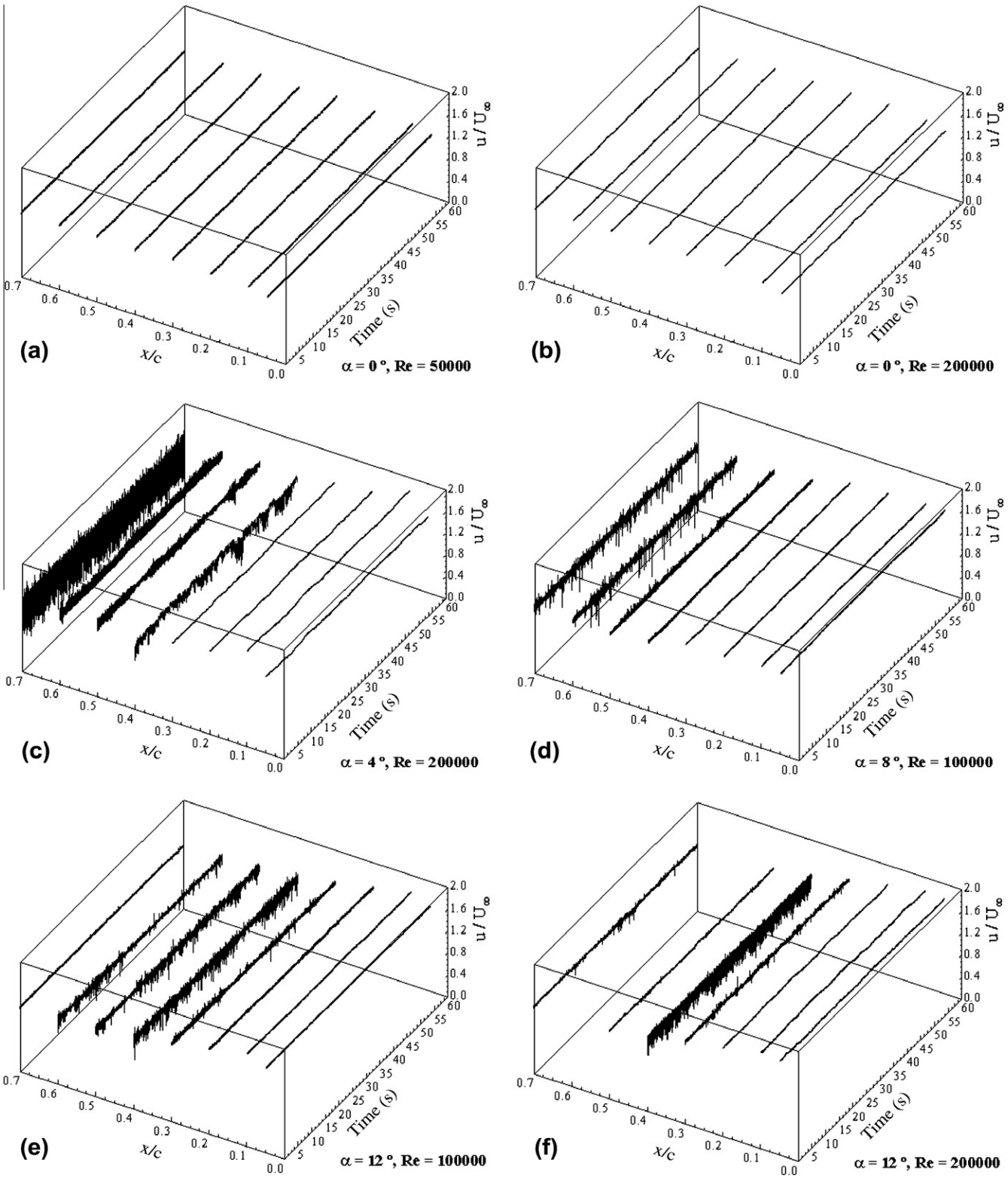

Fig. 14. Time-dependent velocity fluctuations over the NACA2415 aerofoil (a) Re = 0.5 × 10^5 α = 0°, (b) Re = 2 × 10^5α = 0°, (c) Re = 2 × 10^5 α = 4°, (d) Re = 1 × 10^5α = 8°, (e) Re = 1 × 10^5α = 12°, and (f) Re = 2 × 10^5 α = 12°.

themselves felt. As is shown in Fig. 14a and b, the velocity fluctuations are very low at α = 0° and the flow is laminar until *x*/*c* = 0.7. The onset of the transition from laminar to turbulence moves towards the leading edge of the aerofoil as the angle of attack increases at same the Re number: for Re = 2 × 10^5 at 4° (Fig. 14c) this occurs approximately at *x*/*c* = 0.62, at 12° (Fig. 14f) at *x*/*c* = 0.3, for Re = 1 × 10^5 at 8° (Fig. 14d) at nearly *x*/*c* = 0.5, at 12° (Fig. 14e) at *x*/*c* = 0.3. Moreover, as the Re number increases the velocity fluctuations get wider due to the fact that the flow momentum raises as seen from all the graphs. The velocity

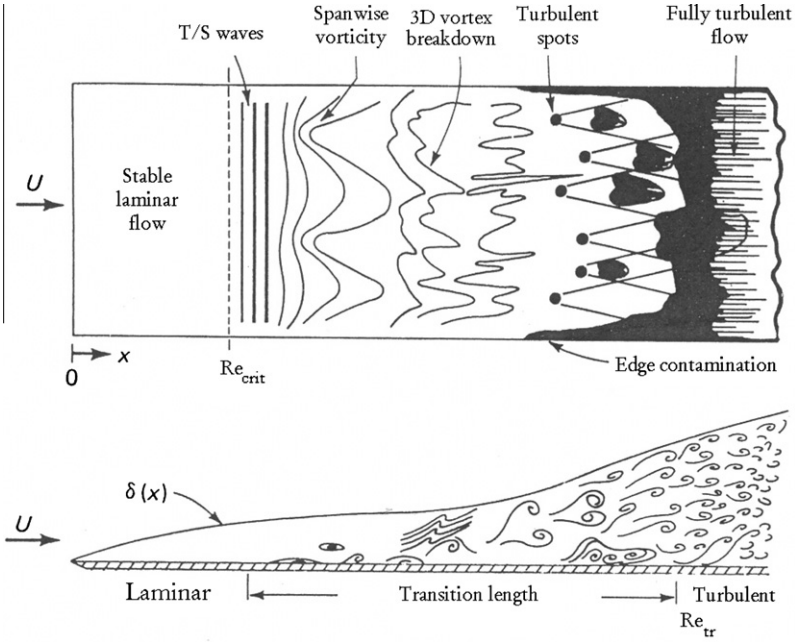

Fig. 15. Schematic of natural transition over the flat plate [31].

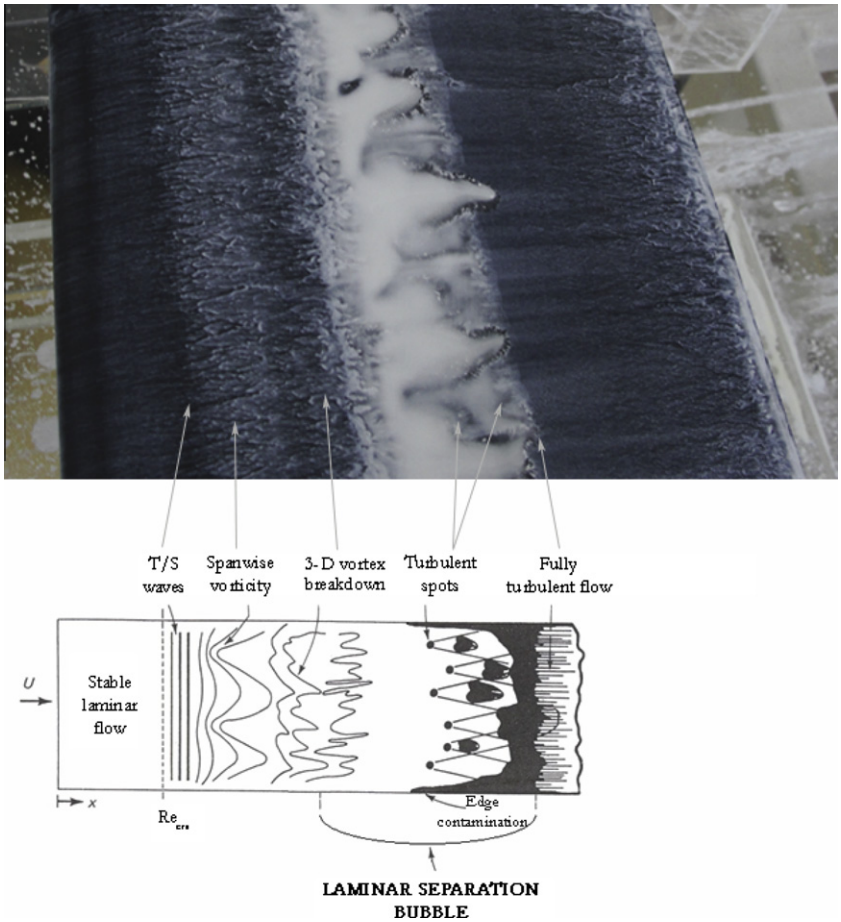

Fig. 16. Comparison of schematic of separation-induced transition process with the experimental photograph obtained oil-flow visualization over the NACA2415 aerofoil at $\alpha = 4^\circ$ at $Re = 3 \times 10^5$.

measurements using the hot-wire system ensure to see the formation of transition, separation and turbulent flow, as observed in the pressure distribution graphs and oil flow visualization photographs. However, as shown in Fig. 14e and f, the velocity fluctuations decrease at $x/c = 0.6$ and $x/c = 0.7$ at $\alpha = 12^\circ$ due to slow circulation velocities of the large vortexes in the separated flow.

3.5. Laminar separation bubble and transition over NACA2415 aerofoil

LSBs can be classified as long and short bubbles. The location and size of the bubble is a function of aerofoil shape, angle of attack, freestream disturbances and Re number [5,30]. The LSB moves forward and contract in streamwise extent by the increase in angle of attack, which is classified as a short bubble [5,30]. Within this kind of bubble, a small region of constant pressure can be seen, which causes a plateau in the curve of pressure distribution. Then the curve of pressure distribution recovers in consequence of reattachment. As the angle of attack increases further, the separation point continues to move towards the leading edge and at a certain angle of attack the flow can no longer reattach to the aerofoil surface within a short distance. This phenomenon is called breakdown or burst of bubble. The occurrence of the breakdown phenomenon does not lead the flow to separate completely. The separated flow passes above the aerofoil and reattaches farther downstream. The flow region under the separated flow slowly circulates and is called dead-air region or a long bubble. The presence of a short bubble does not significantly alter the peak suction. However, the presence of a long bubble results in a suction plateau of reduced levels in pressure distribution over the region occupied by the long bubble and does not result with a sharp suction peak. In this study, long bubble was seen at the angle of attack of 12° and $Re = 0.5 \times 10^5$ (Fig. 9a), this situation also indicates the bursting of the short bubble, which leads to form the long bubble. The pressure distributions of the other cases, in which sharp suction peaks can be seen, indicate the presence of the short bubbles.

The schematic of idealized natural transition phenomena on the flat plate described in the book of White [31] was given in Fig. 15. In boundary layers with free-stream turbulence intensities of 1% or less, the natural transition occurs [15,32]. In the natural transition, Tollmien/Schlichting (T/S) waves occurred due to the fact that a shear layer increase the viscous instability, is firstly appeared inside the boundary layer as elongated streaky structures. The streaky structure is started to disrupt (spanwise vorticity), and then three dimensional vortex breakdown is occurred as a random disruptions. As the flow moves on the surface, intense randomized flow and turbulent spots is shown. The turbulent spots grow in size and merge until the flow is fully turbulent.

Another important transition mechanism is separation-induced transition [33], where a laminar boundary layer separates under the influence of a pressure gradient and transition develops within the separated shear layer. When a laminar boundary layer separates, transition occurs in the separated flow. The energized flow in which transition from laminar to the turbulent occurs reattaches. This reattachment forms a LSB on the surface [32]. In this study, this transition process was observed in the oil flow visualization photograph over the suction surface of the NACA2415 aerofoil as given in Fig. 16. And also, in this figure the separation-induced transition was represented by rearranging the figure of the natural transition in the book of White [31] as an analogy, because of the fact that there is no representative figure of separated-induced transition in the literature. As it can be seen in the rearranged figure the LSB formed between three dimensional vortex breakdown and fully turbulent flow on the suction surface of the NACA2415 aerofoil. Turbulent spots which exist in the transitional zone and LSB [32] are also indicated in the figure. The turbulent spots grew in size, and then they agglomerated. After the agglomeration of the turbulent spots the flow became fully turbulent following the transition, which caused the separated-flow to reattach and the LSB to form.

Fig. 17 illustrates the experimental photograph obtained from oil-flow visualization and the results of velocity fluctuations and C_P distribution over the NACA2415 aerofoil at the angle of attack of 4° at $Re = 2 \times 10^5$. The accumulated region of pigments shows

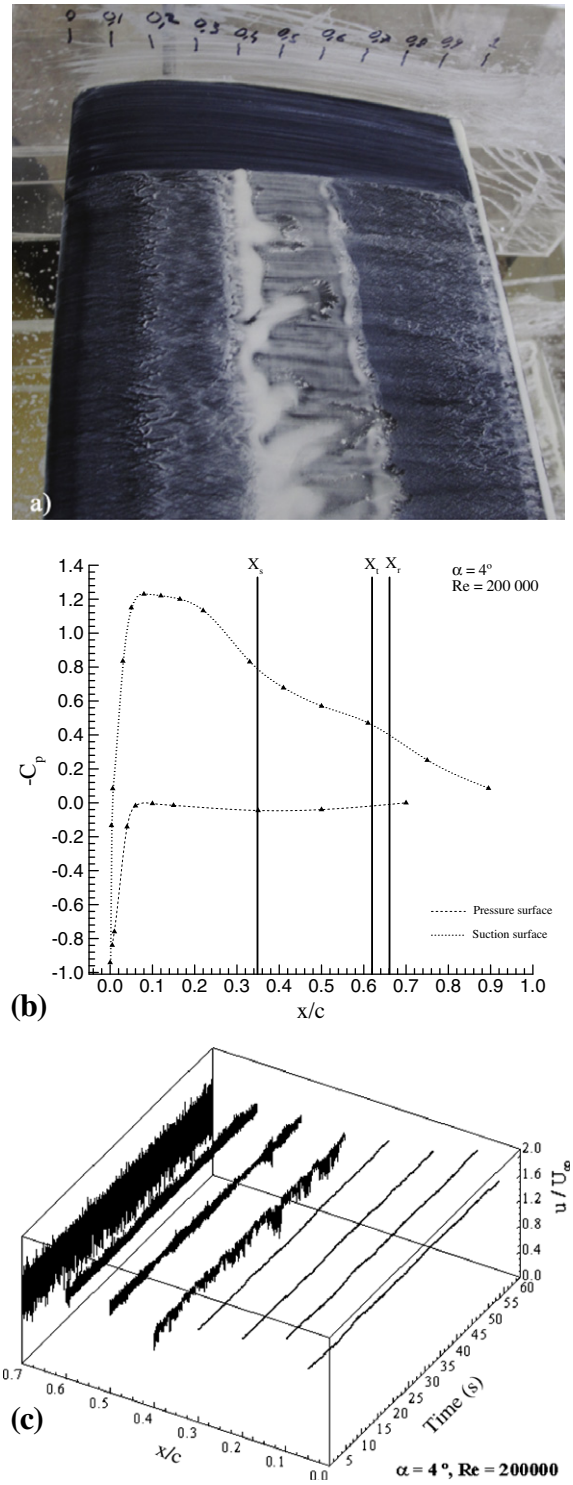

Fig. 17. Comparison of the experimental photograph obtained oil-flow visualization with velocity fluctuation and pressure distribution over the NACA2415 aerofoil ($\alpha = 4°$, $Re = 2 \times 10^5$).

where the flow has decelerated to a near stagnant state, which correlates with the point at which the pressure gradient cancels out causing separation ($x/c = 0.35$). Between $x/c = 0.4$ and $x/c = 0.6$, the intense randomized separated flow is shown in the results of the velocity fluctuations, and the transition from laminar to turbulence occurs approximately at $x/c = 0.62$ and the turbulent flow reattached at $x/c = 0.66$ as observed in the photograph of the oil flow visualization results.

4. Conclusions

In this study, the LSB, transition and reattachment formed over the NACA2415 aerofoil at low Re numbers were experimentally investigated in order to gain some understanding for low Re number aerodynamics of the NACA2415 aerofoil. In the investigation of the pressure distributions, the formation and progress of the LSB, transition and re-attached flow were seen obviously. Also, the graphs of the pressure coefficient ensured to see the transition from laminar to turbulent occurred just after highest point of the peak in the pressure coefficient curve of suction surface. In the figures of the force and moment, the fluctuations pointed out the separation at post-stall. The $C_L - \alpha$ curves showed that the stall angle increased and the stall abruptness decreased as Reynolds number raised. More detailed investigation made by using the oil-flow visualization method. In the oil-flow visualization and pressure distribution experiments, it was concluded that as the angle of attack increased the separation point moves towards the leading edge at all Re numbers. Furthermore, the formation and progress of the separation bubble and re-attached flow were observed clearly in the oil-flow visualization, pressure distribution and velocity measurements. It was concluded from the oil-flow visualization results that at lower Re numbers, short bubble burst at higher angles of attack, which caused long bubble to occur.

Acknowledgments

The authors would like to acknowledge funding from the Scientific and Technological Research Council of Turkey (TÜBİTAK) under the Project no: 110M068, the Scientific Research Projects Unit of Erciyes University under the contract no: FBA-10-3355, FBY-10-3369, FBY-11-3516. They would also like to thank personally M. Tuğrul AKPOLAT for his contributions to this paper.

References

[1] R. Ricci, S.A. Montelpare, Quantitative IR thermographic method to study the laminar separation bubble phenomenon, International Journal of Thermal Sciences 44 (2005) 709–719.
[2] R. Ricci, S.A. Montelpare, E. Silvi, Study of acoustic disturbances effect on laminar separation bubble by IR thermography, Experimental Thermal and Fluid Science 31 (2007) 349–359.
[3] W. Zhang, R. Hain, C.J. Kahler, Scanning PIV investigation of the laminar separation bubble on a SD7003 airfoil, Experiment in Fluids 45 (2008) 725–743.
[4] M. Gaster, The structure and behaviour of separation bubbles, Aeronautical Research Council Reports and Memoranda, No: 3595, London, 1967.
[5] I. Tani, Low speed flows involving bubble separations, Progress in Aerospace Sciences 5 (1964) 70–103.
[6] K. Rinioie, N. Takemura, Oscillating behaviour of laminar separation bubble formed on an aerofoil near stall, The Aeronautical Journal 108 (2004) 153–163.
[7] A.C.N. Tan, J.D. Auld, Study of Laminar Separation Bubbles at Low Reynolds Number under Various Conditions 11th Australasian Fluids Mechanics Conference, 1992, University of Tasmania, Hobart, Australia.
[8] M.S. Sharma, K. Poddar, Experimental investigation of laminar separation bubble for a flow past an airfoil, in: Proceedings of ASME Turbo Expo 2010: Power for Land, Sea, and Air (GT2010) June 1418, 2010, Glasgow, UK.
[9] S.S. Diwan, O.N. Ramesh, Laminar separation bubbles: dynamics and control, SADHANA – Academy Proceedings in Engineering Science 32 (2007) 103–109.
[10] Z. Yang, L.F. Haan, H. Hui, An experimental investigation on the flow separation on a low-Reynolds number airfoil, in: 45th AIAA Aerospace Sciences Meeting and Exhibit, 2007, Reno Nevada.
[11] R. Hain, C. Kahler, J. Radespiel, Dynamics of laminar separation bubbles at low Reynolds number aerofoils, Journal of Fluid Mechanics 630 (2009) 129–153.
[12] S. Burgmann, C. Briicker, W. Shroder, Scanning PIV measurements of a Laminar separation bubble, Experiments in Fluids 41 (2006) 319–326.
[13] C.P. Haggmark, C. Hildings, D.S. Henningson, A numerical and experimental study of a transitional separation bubble, Aerospace Science and Technology 5 (2001) 317–328.
[14] M. Lang, U. Rist, S. Wagner, Investigations on controlled transition development in a laminar separation bubble by means of LDA and PIV, Experiments in Fluids 36 (2004) 43–52.
[15] L. Brandt, P. Schlatter, D.S. Hennngson, Transition in boundary layers subject to free-stream turbulence, Journal of Fluid Mechanics 517 (2004) 167–198.
[16] L. Brandt, C. Cossu, J.M. Chomaz, P. Huerre, D.S. Henningson, On the convectively unstable nature of optimal streaks in boundary layers, Journal of Fluid Mechanics 485 (2003) 221–242.
[17] L. Brandt, D.S. Henningson, Transition of streamwise streaks in zero-pressure-gradient boundary layers, Journal of Fluid Mechanics 472 (2002) 229–262.
[18] L. Brandt, D.S. Henningson, D. Ponziani, Weakly non-linear analysis of boundary layer receptivity to free-stream disturbances, Physics in Fluids 14 (2002) 1426–1441.
[19] M.S. Genç, Ü. Kaynak, H. Yapici, Performance of transition model for predicting low Re aerofoil flows without/with single and simultaneous blowing and suction, European Journal of Mechanics B/Fluids 30 (2011) 218–235.
[20] M.S. Genç, Numerical simulation of flow over an thin aerofoil at high Re number using a transition model, Proceedings of the IMechE, Part C – Journal of Mechanical Engineering Science 224 (2010) 2155–2164.
[21] M.S. Genç, Control of Low Reynolds Number Flow over Aerofoils and Investigation of Aerodynamic Performance (in Turkish), Ph.D Thesis, Graduate School of Natural and Applied Sciences, 2009, Erciyes University, Kayseri, Turkey.
[22] M.S. Genç, Ü. Kaynak, G.D. Lock, Flow over an aerofoil without and with leading edge slat at a transitional Reynolds number, Proceedings of the IMechE, Part G – Journal of Aerospace Engineering 223 (2009) 217–231.
[23] M.S. Genç, G. Lock, Ü. Kaynak, An experimental and computational study of low Re number transitional flows over an aerofoil with leading edge slat, in: 8. AIAA Aviation Technology, Integration and Operations Conference, ATIO 2008, Anchorage, Alaska, USA.
[24] İ. Karasu, Experimental and numerical investigations of transition to turbulence and laminar separation bubble over aerofoil at low Reynolds number flows (In Turkish), MSc. Thesis, Graduate School of Natural and Applied Sciences, Erciyes University, Kayseri, Turkey, 2011.
[25] S.J. Schreck, N.N. Sorensen, M.C. Robinson, Aerodynamic structures and processes in rotationally augmented flow fields, Wind Energy 10 (2007) 159–178.
[26] T.Y. Chen, L.R. Liou, Blockage corrections in wind tunnel tests of small horizontal-axis wind turbines, Experimental Thermal and Fluid Science 35 (2011) 565–569.
[27] W. Merzkirch, Flow Visualization, Academic Press Inc. Ltd., London, 1974.
[28] D.F. Perrens, Flow visualisation in low speed wind tunnels, Physics in Education 5 (5) (1970) 262–265.
[29] E.C. Holland, Leading-edge slat for NACA2415 aerofoil, Final year project AA9, University of Bath, 2007.
[30] K.M. Swift, An Experimental Analysis of the Laminar Separation Bubble at Low Reynolds Numbers, Master's Thesis, University of Tennessee, Knoxville, 2009.
[31] F.M. White, Viscous fluid flow, second ed., McGraw-Hill Inc., New York, 1991.
[32] R.E. Mayle, The role of laminar-turbulent transition in gas turbine engines, Journal of Turbomachinery 113 (1991) 509–537.
[33] R.E. Mayle, Transition in a separation bubble, ASME Journal of Turbomachinery 118 (1996) 752–759.